Axogenic mechanism enhances retinal ganglion cell excitability during early progression in glaucoma

Michael L. Risner[a,1], Silvia Pasini[a,1], Melissa L. Cooper[a], Wendi S. Lambert[a], and David J. Calkins[a,2]

[a]Department of Ophthalmology and Visual Sciences, Vanderbilt University Medical Center, Nashville, TN 37232-0654

Edited by Donald J. Zack, Johns Hopkins University, Baltimore, MD, and accepted by Editorial Board Member Jeremy Nathans January 9, 2018 (received for review August 22, 2017)

Diseases of the brain involve early axon dysfunction that often precedes outright degeneration. Pruning of dendrites and their synapses represents a potential driver of axonopathy by reducing activity. Optic nerve degeneration in glaucoma, the world's leading cause of irreversible blindness, involves early stress to retinal ganglion cell (RGC) axons from sensitivity to intraocular pressure (IOP). This sensitivity also influences survival of RGC dendrites and excitatory synapses in the retina. Here we tested in individual RGCs identified by type the relationship between dendritic organization and axon signaling to light following modest, short-term elevations in pressure. We found dendritic pruning occurred early, by 2 wk of elevation, and independent of whether the RGC responded to light onset (ON cells) or offset (OFF cells). Pruning was similarly independent of ON and OFF in the DBA/2J mouse, a chronic glaucoma model. Paradoxically, all RGCs, even those with significant pruning, demonstrated a transient increase in axon firing in response to the preferred light stimulus that occurred on a backdrop of generally enhanced excitability. The increased response was not through conventional presynaptic signaling, but rather depended on voltage-sensitive sodium channels that increased transiently in the axon. Pruning, axon dysfunction, and deficits in visual acuity did not progress between 2 and 4 wk of elevation. These results suggest neurodegeneration in glaucoma involves an early axogenic response that counters IOP-related stress to excitatory dendritic architecture to slow progression and maintain signaling to the brain. Thus, short-term exposure to elevated IOP may precondition the neural system to further insult.

neurodegeneration | glaucoma | retinal ganglion cells | axonopathy | dendritic pruning

Identifying new therapeutic targets for neurodegenerative disease requires understanding how neurons in targeted tissues respond early to stress and whether this response includes adaptive mechanisms to slow pathogenesis. Because axon signaling depends on maintenance of excitatory activity, loss of dendritic excitation could represent a candidate to drive an adaptive or protective response. Glaucomatous optic neuropathy (or glaucoma) is the world's most prevalent cause of irreversible blindness, involving specific degeneration of the retinal ganglion cell (RGC) projection through the optic nerve to the brain (1). Glaucoma's hallmark feature is sensitivity to intraocular pressure (IOP), which conveys stress to the RGC axon as it exits the eye in forming the optic nerve. Models of glaucoma pique this sensitivity by elevating IOP over a range of magnitudes and durations. Such models capture important features of other brain disorders, including early axonopathy, cytoskeletal reorganization, glial remodeling, and elimination of excitatory synapses (1–3).

In inducible glaucoma models, RGC dendritic arbors exhibit pruning with even brief periods of IOP elevation, depending on magnitude (4–7). However, recent evidence in mouse models suggests that the rate of pruning appears to depend on the polarity of the RGC response to light, which varies over the 30 or so types in the mouse retina (8, 9). This response divides into two major classes: excitation by increments of light (ON cells) vs. excitation by decrements (OFF cells); some RGC types respond to both (ON-OFF). This distinction corresponds to a morphological difference in dendritic stratification in the inner synaptic (plexiform) layer of the retina. The dendrites of ON RGCs stratify in the proximal half of the inner plexiform layer (the ON sublamina), and OFF cell dendrites stratify in the distal half (the OFF sublamina); ON-OFF RGCs stratify in both. This distinction may translate to differences in progression. Recent studies suggest that OFF RGCs may be more susceptible to IOP-related dendritic pruning, corresponding to quicker elimination of synapses in the OFF sublamina (5–7).

Our objective here is to evaluate how the mouse retina reacts to glaucomatous stress early in progression by comparing in individual RGCs the physiological light response to dendritic arborization following modest, short-term elevations in IOP. We identified four major types of RGC using morphological, neurochemical, and physiological criteria established in the literature (7, 10–13). Dendritic pruning did not depend on response polarity/dendritic stratification, because ON and OFF dendritic arbors showed significant dendritic reduction by 2 wk of elevation that depended more on RGC type. Pruning was similarly independent of ON and OFF stratification in aged retina of the DBA/2J mouse, a common chronic glaucoma model. Paradoxically, each RGC type demonstrated an enhanced response to the preferred light stimulus, even those types with dendritic pruning. This increase in firing rate was transient, because light response decreased between 2 and 4 wk of elevated IOP. During this

Significance

Identifying new therapies for neurodegenerative disease requires understanding how neurons respond to stress and whether this response includes adaptation to slow progression. Because neurodegeneration affects both axons and dendrites, with their synaptic contacts, adaptation could involve both compartments. We investigated this question in experimental glaucoma, the world's leading cause of irreversible vision loss. Glaucoma attacks retinal ganglion cell neurons and their axons, which comprise the optic nerve. We found that elevations in ocular pressure, a prominent risk factor for glaucoma, caused a paradoxical increase in ganglion cell excitability, including response to light, even in cells with substantial dendritic pruning. This adaptation arose from voltage-dependent mechanisms in the axon and may help maintain signaling to the brain to preserve vision.

Author contributions: M.L.R., S.P., and D.J.C. designed research; M.L.R., S.P., M.L.C., and W.S.L. performed research; M.L.R., S.P., M.L.C., W.S.L., and D.J.C. analyzed data; and M.L.R., S.P., and D.J.C. wrote the paper.

Conflict of interest statement: D.J.C. is a consultant with Sustain Biotechnology.

This article is a PNAS Direct Submission. D.J.Z. is a guest editor invited by the Editorial Board.

[1]M.L.R. and S.P. contributed equally to this work.

[2]To whom correspondence should be addressed. Email: david.j.calkins@vanderbilt.edu.

This article contains supporting information online at www.pnas.org/lookup/suppl/doi:10.1073/pnas.1714888115/-/DCSupplemental.

Published online February 20, 2018.

transient phase, conventional AMPA receptor-mediated glutamatergic signaling remained constant despite dendritic pruning, possibly through increased presynaptic active zones. However, isolating AMPA receptor signaling eradicated the enhanced light response, which depended on activation of voltage-sensitive sodium channels (NaV). Localization of the NaV1.6 subunit, which supports higher rates of action potential generation (14, 15), increased during the transient phase in the unmyelinated axon segment, including within varicosities that increased in density, size, and proximity to the RGC body with elevated IOP. Antagonism of NaV1.6 suppressed enhancement. Dendritic pruning, axon dysfunction, and deficits in visual acuity did not progress further between 2 and 4 wk of elevation following transient enhancement. Thus, early progression in glaucoma involves a compensatory or preconditioning mechanism that includes an axogenic response to counter IOP-dependent challenges to excitatory dendritic architecture and help RGCs maintain signaling to the brain.

Results

Dendritic Pruning in Glaucoma Affects both ON and OFF RGC Types. We elevated IOP in mice using microbead occlusion of anterior fluid (16–18). An injection raised IOP compared with control for either 2 wk (32%, $P < 0.001$) or 4 wk (26%, $P < 0.001$). We identified first αON-sustained (αON-S) RGCs (Fig. 1*A*). These cells have large cell bodies (area ≥ 180 μm^2), a signature sustained response to light, strong expression of staining for nonphosphorylated neurofilament H protein (SMI32), and narrow dendritic ramification in the ON sublamina relative to bands of choline acetyltransferase (ChAT; Fig. S1 *A* and *B*) (7, 9, 10, 13, 19). Compared with control, the dendritic arbors of αON-S RGCs appeared to diminish in size and complexity by 2 wk of elevated IOP (Fig. 1*B*). When quantified using Sholl analysis, even this brief elevation in IOP significantly reduced dendritic complexity (Fig. 1*C*). This involved decreased mean dendritic field area, which diminished by 35% on average, and total dendrite length, which diminished by 23%, compared with control ($P \leq 0.05$; Fig. 1*D*). Pruning did not progress between 2 and 4 wk of elevated IOP, with indications of modest recovery in both field size and dendrite length (Fig. 1*D*).

Next we identified a type of RGC with dual dendritic arbors in the ON and OFF sublaminas (Fig. 2 *A* and *B*). This RGC is distinguished by lack of staining for SMI32 (11), a characteristic transient response to both onset and offset of light, and narrow dendritic stratification near bands of ChAT (Fig. S1 *C* and *D*). Based on morphology and light response, these likely correspond to the directional selective RGC type identified in other studies (12, 20). The reconstructed dendritic arbors of ON-OFF RGCs appeared to diminish in size by 2 wk of elevation, but only in the ON sublamina (Fig. 2*B*). Sholl analysis of complexity for ON dendrites demonstrated significant pruning within a 120- to 230-μm radius from the soma, which, like αON-S RGCs, did not progress between 2 and 4 wk of elevated IOP (Fig. 2*C*). Pruning at 2 wk corresponded to a decrease in both mean dendritic field area (59%) and total dendrite length (32%) compared with control RGCs of the same type (Fig. 1*D*; $P = 0.02$). Neither measure progressed between 2 to 4 wk; both ON arbor size and dendrite length at 4 wk did not differ from control RGCs ($P \geq 0.07$). In contrast to ON dendrites, elevated pressure had little influence on complexity of the dendritic arbor in the OFF sublamina (Fig. 2*E*), without a significant decline in dendritic field area or total length (Fig. 2*F*).

The results for ON-OFF RGCs suggest that ON arbors rather than OFF are more susceptible to IOP early in progression. To test this, we identified two types of OFF αRGC (Fig. S2), again based on dendritic stratification, response to light offset, large cell bodies (area ≥ 180 μm^2), and expression of nonphosphorylated neurofilament (7, 10). Unlike their ON counterparts, αOFF-S RGC cells showed very little change in dendritic complexity with elevated IOP (Fig. S3). However, the dendritic arbors of αOFF-transient (αOFF-T) RGCs demonstrated dramatically reduced size and complexity following 2 wk of elevated IOP (Fig. S4). We also found similar pruning for ON, OFF, and ON-OFF RGCs in the DBA/2J mouse (Figs. S5 and S6), which develops a glaucoma-like phenotype over a period of months as they age (21–23).

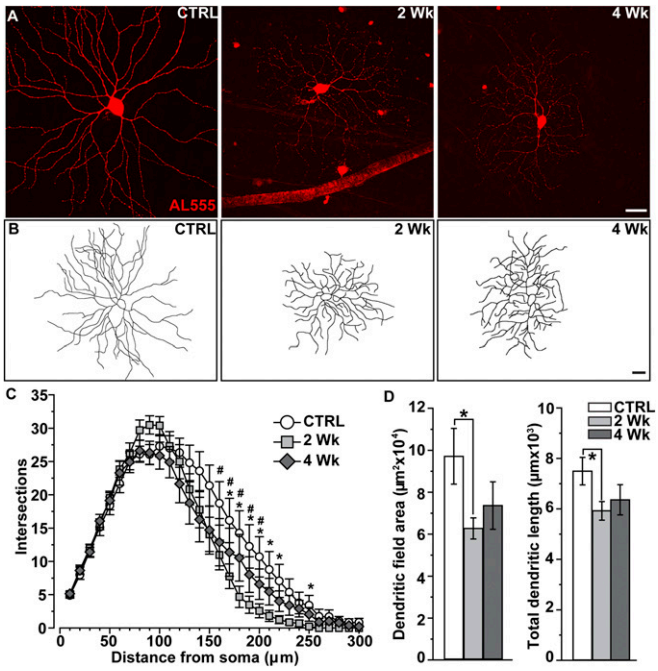

Fig. 1. Early pruning of αON-sustained RGC dendrites. (*A*) Confocal micrographs of αON-S RGCs following intracellular filling with Alexa 555 dye (AL555) in control (CTRL) retinas and from retinas following 2 wk and 4 wk of elevated IOP (26–32%). (*B*) Reconstructed dendritic arbors show shrinkage after 2 wk of elevated IOP. (Scale bars: *A* and *B*, 40 μm.) (*C*) Sholl analysis averaged across αON-S RGCs from CTRL ($n = 16$), 2 wk ($n = 11$), and 4 wk ($n = 14$) retinas shows number of dendritic intersections across concentric rings at regular distances from the soma. After 2 wk of elevated IOP, dendritic intersections decreased significantly within a radius of 170–220 and 250 μm from the soma compared with CTRL (*$P \leq 0.04$, two-way ANOVA); 4-wk cells also showed significant loss of complexity at similar distances ($^{\#}P \leq 0.03$, two-way ANOVA). (*D*) Dendritic field area and total dendrite length both decrease for 2 wk αON-S RGCs compared with CTRL cells (*, area: $P = 0.03$, *t* test; length: $P = 0.02$, *t* test), but recover slightly in the 4-wk group. Data: mean ± SEM. Statistical analysis as described in *Methods*.

Paradoxical Transient Increase in Excitability Accompanies Dendritic Pruning. Next, we measured how IOP influences the response to the preferred light stimulus for RGCs characterized morphologically. The αON-S RGCs we examined (Fig. 1) responded to light with a sustained train of action potentials for the duration of the stimulus (Fig. 3*A*), following the pattern of inward current (Fig. S1*A*). Two weeks of elevated IOP appeared to increase depolarization of the resting membrane potential as well as firing rate to the preferred stimulus (Fig. 3*A*, *Center*). The average light response measured demonstrated a sharp, transient peak followed by the sustained component (Fig. 3*B*), again following the profile of the inward current (Fig. S1). Two weeks of elevated IOP increased the pattern of light-induced excitability, despite significant pruning of the dendritic arbor in the ON sublamina (Fig. 1). Accordingly, compared with control cells, the mean response rate over the duration of the light stimulus increased significantly after 2 wk of elevated pressure (30.2 ± 1.9 vs. 20.6 ± 1.5 spikes/s; $P < 0.001$; Fig. 3*C*, *Left*). Indeed, the median firing

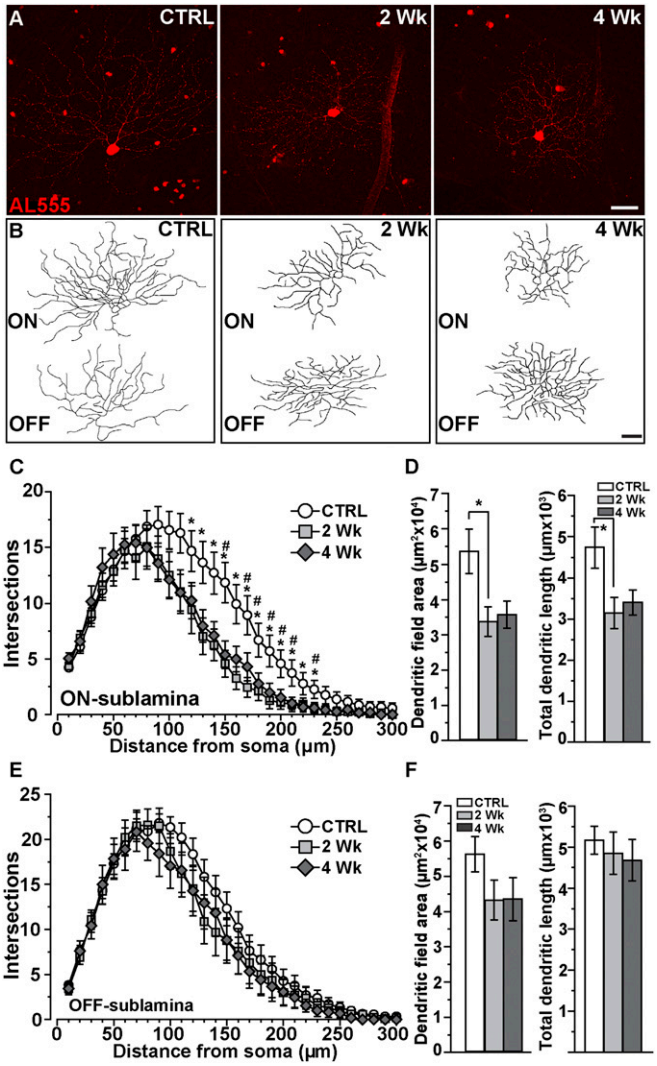

Fig. 2. ON sublamina dendrites for ON-OFF RGCs are targeted early. (*A*) ON-OFF RGCs following intracellular filling (AL555) from CTRL, 2-wk, and 4-wk retinas. (*B*) Reconstructions indicate shrinkage in the ON sublamina with elevated IOP. (Scale bars: *A* and *B*, 40 μm.) (*C*) Sholl analysis averaged from CTRL ($n = 24$), 2 wk ($n = 15$), and 4 wk ($n = 12$) RGCs show complexity reduces at 2 wk within a radius of 120–230 μm from the soma compared with CTRL (*$P \leq 0.03$, two-way ANOVA). These reductions remained significant after 4 wk for about the same radius (150, 170–210, and 230 μm; #$P \leq 0.04$, two-way ANOVA). (*D*) Reduced complexity corresponded to smaller ON dendritic fields with decreased total dendrite length for 2-wk cells (*, area: $P = 0.03$, *t* test; length: $P = 0.02$, *t* test). (*E*) Sholl analysis of OFF dendritic arbors shows only minor changes for both 2- and 4-wk ON-OFF RGCs that were not significant at any distance from the soma ($P = 0.23$, two-way ANOVA); neither field area nor total length declined significantly (*F*; area: $P = 0.25$, *t* test; length: $P = 0.48$, *t* test). Data: mean ± SEM.

rate for 2-wk cells increased from 12.5 to 28.3 spikes/s ($P < 0.001$), and the integrated response defined by the area under the curve for firing rate during the light stimulus also tended to increase (Fig. 3*C*, *Center*). This increase accompanied a significant increase in depolarization of the resting membrane potential from −58.4 ± 1.1 mV for control to −52.9 ± 1.7 mV for 2-wk cells ($P = 0.007$; Fig. 3*C*, *Right*). This increase in excitability for αON-S RGCs was transient, because for 4-wk cells the response profile diminished (Fig. 3*B*) and the mean firing rate decreased by 70% (6.2 spikes/s) compared with control cells ($P < 0.001$; Fig. 3*C*). Although the integrated response to light also tended to diminish ($P = 0.07$), resting membrane potential returned to control cell levels ($P = 0.12$; −55.1 ± 1.8 mV).

The ON-OFF RGCs described in Fig. 2 demonstrated a transient burst of action potentials both at the onset and offset of the light stimulus (Fig. 3*D*), each corresponding to transient inward current as shown (Fig. S1*C*). Two weeks of elevated IOP increased the response to light onset in both magnitude and duration (Fig. 3*E*). Like αON-S RGCs, this increase occurred despite significant pruning of the dendritic arbor in the ON sublamina (Fig. 2). Accordingly, compared with control cells, the mean response rate over the duration of the light stimulus nearly doubled after 2 wk of elevated pressure (4.6 ± 0.6 vs. 2.6 ± 0.4 spikes/s; $P < 0.001$; Fig. 3*F*). Like αON-S RGCs, this increase was transient, because for 4-wk ON-OFF RGCs the mean firing rate to light onset decreased by 38% compared with control cells of the same type (1.6 ± 0.4 spikes/s; $P = 0.001$). This corresponded to a significant decrease in the integrated ON response for 4-wk cells ($P = 0.03$), whereas 2-wk cells demonstrated a modest increase (Fig. 3*G*). The OFF response to light was unchanged for both 2 and 4 wk of elevated IOP, as were the dendrites in the OFF sublamina (Fig. 2).

Like their ON counterparts, αOFF-S RGCs respond to their preferred light stimulus with a sustained volley of action potentials (Fig. 4*A*), but in this case to the offset of light. This too follows the pattern of inward current (Fig. S2). However, unlike αON-S RGCs, αOFF-S RGCs did not demonstrate appreciable dendritic pruning with elevated IOP (Fig. S3). Even so, 2 wk of elevated IOP enhanced the average αOFF-S RGC response to its preferred stimulus (Fig. 4*B*), as it did for αON-S RGCs. The mean firing rate at light offset nearly doubled compared with control cells (13.0 ± 0.9 vs. 7.3 ± 0.6 spikes/s, $P < 0.001$; Fig. 4*C*). Like the other cell types we examined, the increased average response was transient, because 4 wk of elevated IOP nearly halved the mean firing rate compared with control ($P < 0.001$; Fig. 4*C*). The integrated response to light tended to reflect these changes (Fig. 4*C*, *Center*). Like their ON counterparts, αOFF-S RGCs also demonstrated a more depolarized resting membrane potential compared with control cells: −52.1 ± 1.3 vs. −57.5 ± 1.0 mV, $P = 0.005$; Fig. 4*C*, *Right*). Similarly, αOFF-T RGCs cells also respond to light offset, but with a transient burst of action potentials that quickly dissipates (Fig. 4*D*). Interestingly, although 2 wk of elevated IOP dramatically reduced their dendritic arbors (Fig. S4), the average response of αOFF-T RGCs to their preferred stimulus did not diminish (Fig. 4 *E* and *F*). However, by 4 wk, the mean firing rate decreased by over half compared with control ($P = 0.03$; Fig. 4*F*). Accordingly, the mean integrated response during light offset also diminished for 4-wk cells ($P = 0.04$). Although the peak firing rate at 2 wk increased modestly compared with control cells (20.6 ± 2.5 vs. 13.5 ± 2.8 spikes/s, respectively; $P = 0.07$), the response to light offset was significantly faster (Fig. 4*E*, *Inset*). Two weeks of elevation reduced time to the first action potential by 36% compared with control: 94.8 ± 4.8 vs. 148.3 ± 13.1 ms, respectively ($P = 0.03$; Fig. 4*F*). This change too was transient, returning to control by 4 wk ($P = 0.20$).

Thus, no RGC type we examined demonstrated a reduced response to its preferred light stimulus after 2 wk of elevated IOP, even for those cells with dendritic pruning within that time (αON-S, ON-OFF, and αOFF-T). Rather, for each type, elevated IOP led to transient enhancement of excitability by multiple measures that varied in significance between RGC types. To determine more accurately how enhancement generalizes across types and IOP exposures, we normalized each physiological parameter for each RGC type by the mean value for the corresponding control cell and pooled the data according to IOP. When normalized in this way, RGCs exposed to 2 wk of elevated IOP demonstrated significantly increased mean (+60%, $P = 0.005$) and peak (+39%, $P = 0.007$) firing rates and integrated response (+71%, $P = 0.005$) to the preferred light stimulus

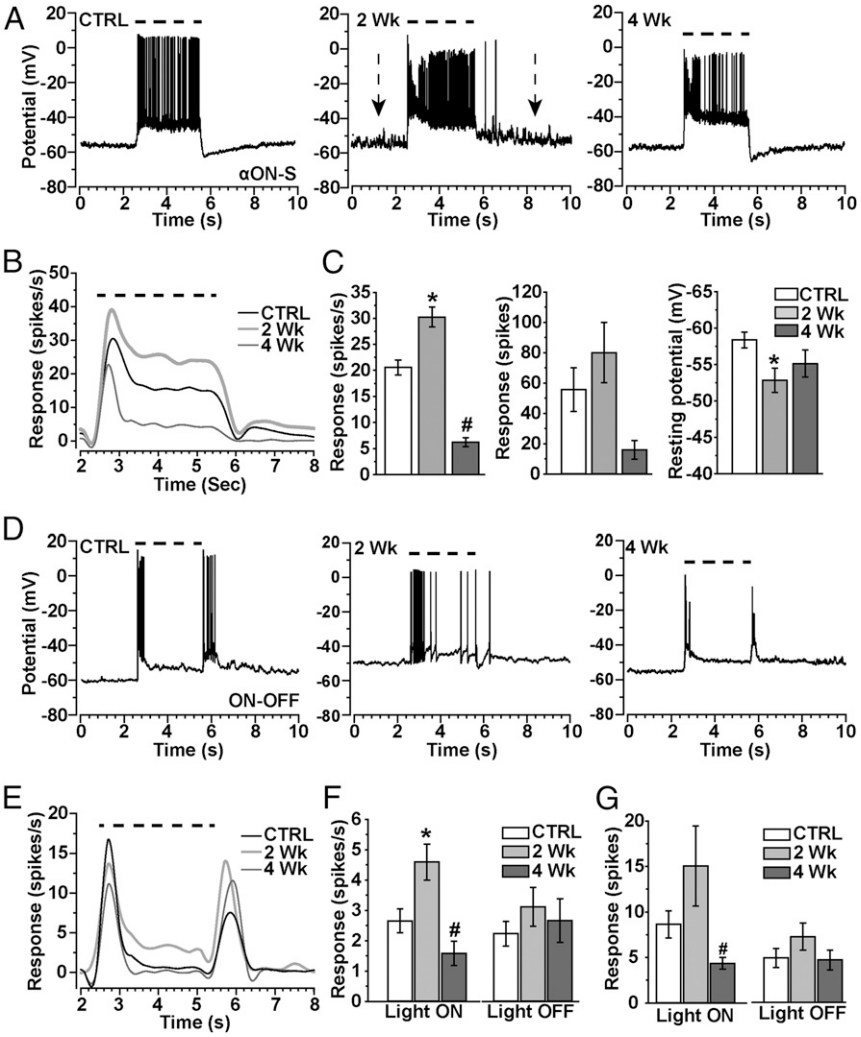

Fig. 3. Transient increase in light response accompanies dendritic pruning. (*A*) Whole-cell current-clamped recordings (0 pA) of voltage response before, during, and after a 3-s light exposure (dashed line) for αON-S RGCs from CTRL, 2-wk, and 4-wk retinas. Resting membrane potential appears to increase for 2-wk cells (arrows). (*B*) Mean voltage firing rate (spikes/s) to light stimulus (dashed line) averaged for CTRL (18), 2-wk (15), and 4-wk (13) αON-S RGCs. (*C*, *Left*) Mean response rate (spikes/s) during the light stimulus increases for 2-wk RGCs ($^{*}P = 0.04$) but decreases for 4-wk cells ($^{\#}P < 0.001$) compared with CTRL. (*C*, *Center*) Integrated response (spikes) for αON-S RGCs during light stimulus shows a modest increase for 2-wk cells and a decrease for 4-wk cells, and mean resting potential becomes more depolarized for 2-wk cells (*Right*; $^{*}P = 0.007$). (*D*) Current-clamp voltage response to light (dashed line) for CTRL, 2-wk, and 4-wk ON-OFF RGCs shows transient response to light onset and offset. (*E*) Response (spikes/s) to light (dashed line) averaged for CTRL (24 cells), 2-wk (14 cells), and 4-wk (17 cells) ON-OFF RGCs shows increased light-induced activity for 2-wk cells. (*F*, *Left*) Mean response (spikes/s) of ON-OFF RGCs during light stimulus (light ON) and for a fixed interval (5.5–8.5 s) following light offset (light OFF). Response to light significantly increased for 2-wk cells ($^{*}P < 0.001$), but decreased for 4-wk cells ($^{\#}P = 0.001$) compared with CTRL RGCs of the same type. (*G*) Integrated response (spikes) for ON-OFF RGCs during (light ON) and following (light OFF) the stimulus tended to increase for 2-wk cells while significantly decreasing for 4-wk cells ($^{\#}P = 0.03$). The mean integrated response following light offset did not change for either the 2-wk or 4-wk groups compared with CTRL cells ($P = 0.44$). Data: mean ± SEM.

compared with control (Fig. 4 *G–I*). As expected, each of these measures diminishing significantly compared with control cells by 4 wk of elevated IOP ($P \leq 0.02$). Elevated IOP also led to a transient increase in depolarization of resting membrane potential compared with control (+6%, $P < 0.001$; Fig. 4*J*), as well as a quicker response to the preferred stimulus through reduced latency (−24%, $P = 0.006$; Fig. 4*K*). Finally, we noted additional noise in resting membrane potential that accompanied enhanced excitation. For example, αON-S RGCs had a 40% greater coefficient of variance at rest compared with control cells following 2 wk of elevated pressure ($P = 0.03$). This effect can be gleaned from our recordings (Fig. 3*A*). This increase in membrane noise also generalized to all RGCs when normalized by each type's control value ($P = 0.013$; Fig. 4*L*). Resting potential, response latency, and coefficient of variance all returned to control levels by 4 wk of elevated IOP.

Enhanced Light Response Depends on Voltage-Dependent Activity. Our physiological recordings indicate that both ON and OFF RGC types demonstrate transient enhancement in excitability after 2 wk of elevated IOP. This was so even for the three types with early and significant dendritic pruning (Figs. 1 and 2 and Fig. S4). Importantly, enhancement includes a transient increase in response to the preferred light stimulus, which reverses to below control levels by 4 wk (Fig. 4 *G–I*). Next, we sought to understand possible mechanisms underlying this response.

Light-induced excitation of RGCs arises from glutamate released from bipolar cell axon terminals that binds ionotropic receptors localized to postsynaptic dendrites (24). Upon binding glutamate, excitation through AMPA-sensitive glutamate receptors enables activation of voltage-dependent channels that contribute to propagation of depolarization in the RGC (25, 26).

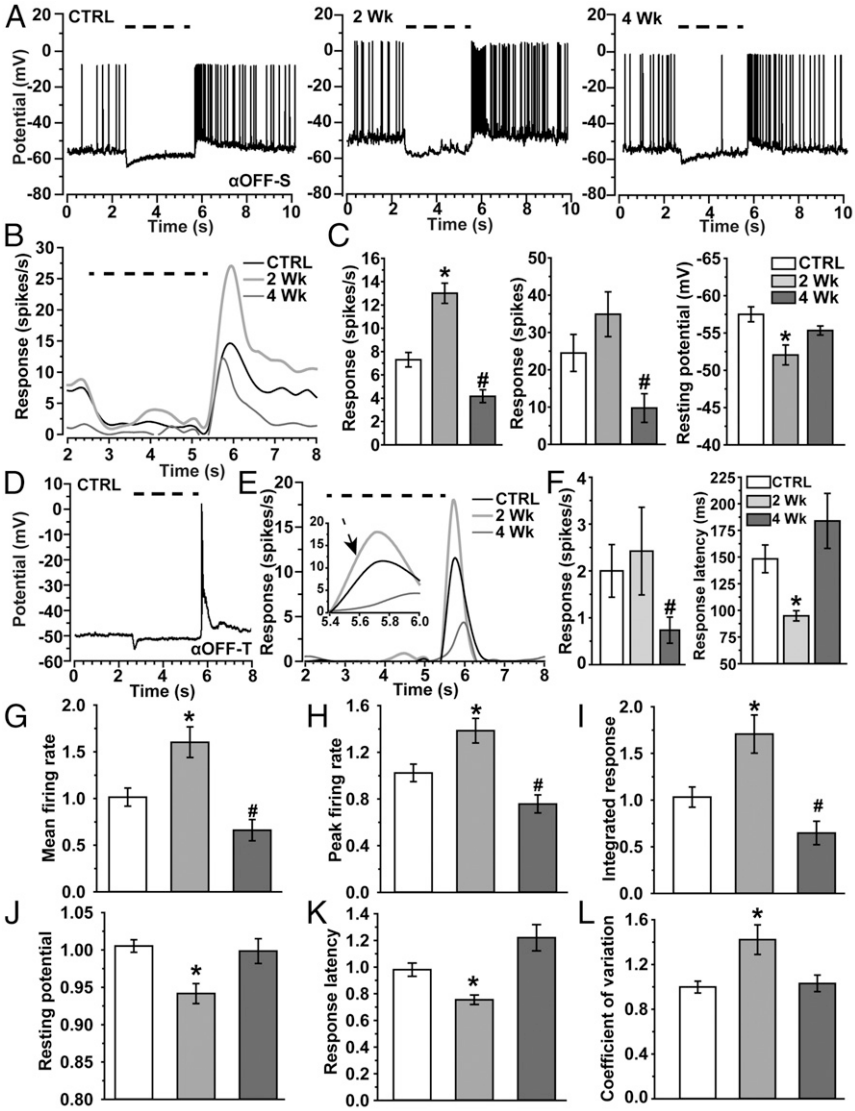

Fig. 4. Enhanced light response generalizes across RGC types. (*A*) Current-clamp voltage response to light (dashed line) for CTRL, 2-wk. and 4-wk αOFF-S RGCs. (*B*) Response (spikes/s) to light (dashed line) averaged for CTRL (12), 2-wk (15), and 4-wk (7) αOFF-S RGCs. (*C*, *Left*) Mean response rate (spikes/s) during a fixed interval (5.5–8.5 s) following light offset (light OFF) increases for 2-wk αOFF-S RGCs ($^{*}P < 0.001$) but decreases for 4-wk cells ($^{\#}P < 0.001$) compared with CTRL cells. (*C*, *Center*) Mean integrated response (spikes) following light offset tended to increase for 2-wk cells ($P = 0.11$) and decreased for 4-wk cells ($^{\#}P = 0.03$). (*C*, *Right*) Mean resting potential becomes more depolarized for 2-wk cells compared with CTRL ($^{*}P = 0.005$). (*D*) Example of the voltage response of αOFF-T RGC (CTRL) to light (dashed line). (*E*) Response (spikes/s) following offset of light (dashed line) averaged for CTRL ($n = 12$), 2-wk ($n = 5$), and 4-wk ($n = 8$) αOFF-T RGCs. *Inset* shows 41% faster rise to peak response for 2-wk cells compared with CTRL (arrow, $P = 0.03$). (*F*, *Left*) Mean response rate (spikes/s) during a fixed interval (5.5–8.5 s) following light offset (light OFF) increased modestly for 2-wk αOFF-T RGCs ($P = 0.07$), but decreased significantly for 4-wk cells ($^{\#}P = 0.03$) compared with CTRL. (*F*, *Right*) Response latency, defined as the time to the first action potential, decreased significantly for 2-wk cells ($^{*}P = 0.05$). (*G*–*L*) Different measurements for ON-OFF, αON-S, αOFF-S, and αOFF-T RGCs normalized with respect to the mean for control cells of same type and then pooled for comparison between IOP groups. By definition, each mean for the control measure is always unity. (*G*) Mean firing rate, (*H*) peak firing rate, and (*I*) integrated response, defined by the area under the curve for firing rate over time, all increase for 2-wk RGCs compared with CTRL ($^{*}P \leq 0.007$); same parameters decrease after 4 wk ($^{\#}P \leq 0.02$). Resting membrane potential (*J*) becomes more depolarized, while response latency (*K*) decreases for 2-wk cells compared with CTRL ($^{*}P \leq 0.006$). Finally, the coefficient of variation (*L*), which represents noise in resting membrane potential, increases for 2-wk cells compared with CTRL ($^{*}P = 0.013$). Data: mean ± SEM, with n = 74–107 (control), 45–107 (2 wk), and 49–66 (4 wk) across measurements.

We isolated pharmacologically the influence of excitatory AMPA receptor signaling in RGCs by silencing other glutamatergic receptors and voltage-gated sodium channels under voltage clamp near the equilibrium potential of chloride to reduce inhibitory currents (27) (Fig. S7). Under these conditions, all four types of RGC both (*i*) failed to demonstrate an enhanced response to the preferred stimulus and (*ii*) did not demonstrate a reduction in response compared with control cells after 2 wk of elevated IOP. For ON-OFF and αOFF-T RGCs, the AMPA-mediated light response did diminish by 4 wk (Fig. S7 *A*–*D*). Finally, the response of αON-S and ON-OFF RGCs to AMPA delivered directly to the cell by puff pipette, which reflects the activity of postsynaptic AMPA receptors (26), decreased progressively between 2 and 4 wk of IOP elevation (Fig. S7*E*). Thus, AMPA receptor-mediated signaling does not underlie the increased light response, because isolating AMPA currents eradicated the increase for each RGC type's preferred stimulus, and delivery of AMPA directly to αON-S and ON-OFF RGCs did, in fact, diminish progressively between

2 and 4 wk of elevated IOP, indicating that dendritic degradation does eventually produce a diminished postsynaptic response.

We asked next what could explain the persistence of the AMPA receptor-mediated contribution to the light response after 2 wk despite dendritic pruning in αON-S, ON-OFF, and αOFF-T RGCs. We found that localization of PSD95, which stabilizes the glutamatergic postsynaptic density on RGC dendrites (24, 28), diminished between 2 and 4 wk of IOP elevation (Fig. S8 *A* and *B*). A presynaptic ribbon marks each glutamatergic active zone in the bipolar cell axon terminal, which can be visualized through immunolabeling for the synaptic ribbon protein RIBEYE (29). Surprisingly, we found that 2 wk of elevated pressure increased RIBEYE significantly (Fig. S8 *C* and *D*). We also found that GABA/glycine-mediated inhibitory currents do not differ between control and 2-wk RGCs (Fig. S8 *G* and *H*).

Our pharmacological experiments indicate that quenching voltage-dependent channels with TTX prevented the enhanced RGC response at 2 wk (Figs. S7 and S8). To explore possible mechanisms of this effect, we examined changes in localization of the voltage-dependent sodium channel NaV1.6, which activates at relatively negative membrane potentials and contributes to action potential initiation and to repetitive firing (15). In mouse retina, NaV1.6 localization within RGCs increased with 2 wk of elevated IOP (Fig. 5 *A* and *D*). Expression seemed to be restricted to somatic and axonal compartments (Fig. 5 *B* and *C*) because labeling was not prominent in the inner plexiform layer where levels remained near control for both 2 ($P = 0.6$) and 4 ($P = 0.5$) wk of elevated IOP (Fig. 5*A*). Interestingly, NaV1.6 localization included intense concentration within axonal varicosities both distal and proximal to the soma; these appeared to increase after 2 wk (Fig. 5*D*). When quantified and normalized to control levels, NaV1.6 increased, significantly only in axons, and then only at 2 wk (Fig. 5*E*). By 4 wk, NaV1.6 channels diminished in both axonal and somatic RGC compartments, including within the varicosities most proximal to the soma (Fig. 5*E*). Perhaps most interesting, the axonal varicosities themselves changed. Two weeks of elevated ocular pressure caused the varicosities along the proximal axon segment to translocate closer to the RGC body, increase in density by 41%, and expand in size (Fig. 5*F*). Finally, we tested how NaV1.6 influences RGC physiology with elevated IOP by measuring the response to light before and after application of the NaV1.6-specific antagonist, 4,9-anhydrotetrodotoxin (aTTX) (30). An independent sample of αON-S (Fig. 5*G*, *Left*) and αOFF (Fig. 5*G*, *Right*) RGCs demonstrated the expected enhanced response after 2 wk of IOP elevation. For CTRL RGCs in each group, both 300 and 500 nM aTTX were equally efficacious in suppressing the preferred light response ($P = 0.99$; Fig. 5*G*). However, for 2-wk RGCs, 300 nM was significantly less effective in suppressing the light current (Fig. 5*G*). The difference in light response between 2-wk and control αON-S RGCs—the enhanced light response—was reduced by 75% by 500 nM aTTX and by 86% after light offset for αOFF RGCs (Fig. 5*G*, *Inset*). When normalized with respect to the degree of suppression for control RGCs and pooled, 300 nM aTTX left a 30% residual preferred light response for 2-wk RGCs ($P < 0.001$), whereas 500 nM was not significantly different from control (Fig. 5*H*).

Enhanced Light Response May Help Slow Axonopathy. A significant element of RGC axon injury in glaucoma is progressive loss of axonal anterograde transport between the retina and superior colliculus (SC), the primary RGC target in rodents (23). Because the transient enhancement of RGC excitation occurs by 2 wk of elevated IOP, we asked if this phenomenon correlates with an axonal outcome at the same time. By 2 wk of elevated IOP, the level of intact transport in the SC degraded by 40% compared with control eyes ($P = 0.018$; Fig. 6 *A* and *B*). Although degradation by 4 wk of elevation was also significant compared with control ($P = 0.008$), deficits in transport did not progress between 2 and 4 wk ($P = 0.24$). For comparison, we also measured the progression of deficits in spatial frequency sensitivity (acuity) by comparing optokinetic tracking (OKT) between control and microbead eyes. Deficits in acuity with elevated IOP occurred very early, with a 7% decline by 3 d post microbead injection that was significant compared with control (Fig. 6*C*). Elevated IOP caused a 27% decrease over 10 d that was interrupted at 2 wk by a significant 25% rebound in acuity that was significant compared with performance at 10 d ($P = 0.02$). Although improvement at 2 wk was transient, following this point acuity did not significantly degrade further compared with 10 d ($P \geq 0.22$).

Discussion

Glaucomatous neurodegeneration involves both an early distal component, affecting RGC axon function in the optic projection (23), and a proximal component involving loss of RGC dendrites and their synapses (31–33). Our fundamental finding is that modestly elevated IOP—the only treatable risk factor in glaucoma—induces a paradoxical increase in RGC light response, even in RGC types with demonstrable dendritic pruning. This enhancement, which is transient, is part of a more general increase in excitability displayed by each of the four types of RGC we identified morphologically and by their characteristic response to a preferred light stimulus (Figs. 1 and 2 and Figs. S1–S4). Dendritic pruning did not depend on response polarity, either to light onset or offset, with both ON and OFF dendrites showing susceptibility depending on RGC type. Enhancement is not through conventional AMPA-sensitive glutamatergic signaling or changes in inhibitory currents, but rather depends on voltage-sensitive sodium channels with the NaV1.6 subunit contributing substantially to the increased light response. This subunit localized mostly in axons, especially within varicosities that increased in size, density, and proximity to the RGC body with elevated pressure. We propose that this axogenic mechanism in the retina boosts RGC excitation even as stress due to IOP challenges conventional glutamatergic signaling.

Ganglion Cell Pruning Is Independent of Response Polarity. An important question in neurodegenerative disease is whether and how certain types of neuron demonstrate increased susceptibility to disease-relevant stressors. Our experiments combining morphological and physiological measurements from single RGCs show 2 wk of moderate (+26%) elevations in IOP induce early pruning of RGC dendritic arbors. This is consistent with previous studies describing dendritic pruning following brief elevations in IOP for some RGC types (6, 7). A key identifier for the 30 or so types is response polarity and dendritic stratification in the corresponding ON or OFF sublamina of the inner plexiform layer (8, 9). Recent evidence suggests that OFF RGCs, in particular αOFF-T RGCs, may be more susceptible to IOP-related stress (5–7). Although accelerated degeneration could be supported through known homotypic coupling between RGCs of this type (34–36), IOP elevation in these studies was far more acute, reaching peaks of 70–88% above control (5–7).

With moderate elevations more typical of human glaucoma (16), we found that pruning was independent of response polarity. Pruning for αON-S RGCs after 2 wk was similar to that of ON-OFF RGCs in the ON sublamina (Figs. 1 and 2). This type of ON-OFF RGC likely corresponds to a directional selective cell identified in previous studies (12, 20). For this RGC, 2 wk of elevation did not influence dendrites in the OFF sublamina, which showed insignificant signs of pruning after even 4 wk (Fig. 2). This result differs from that of El-Danaf and Huberman (6), who found that for anterior motion-selective ON-OFF RGCs, the ON tree expanded slightly, whereas the OFF tree demonstrated modest pruning after 7 d. This difference again could be due to the

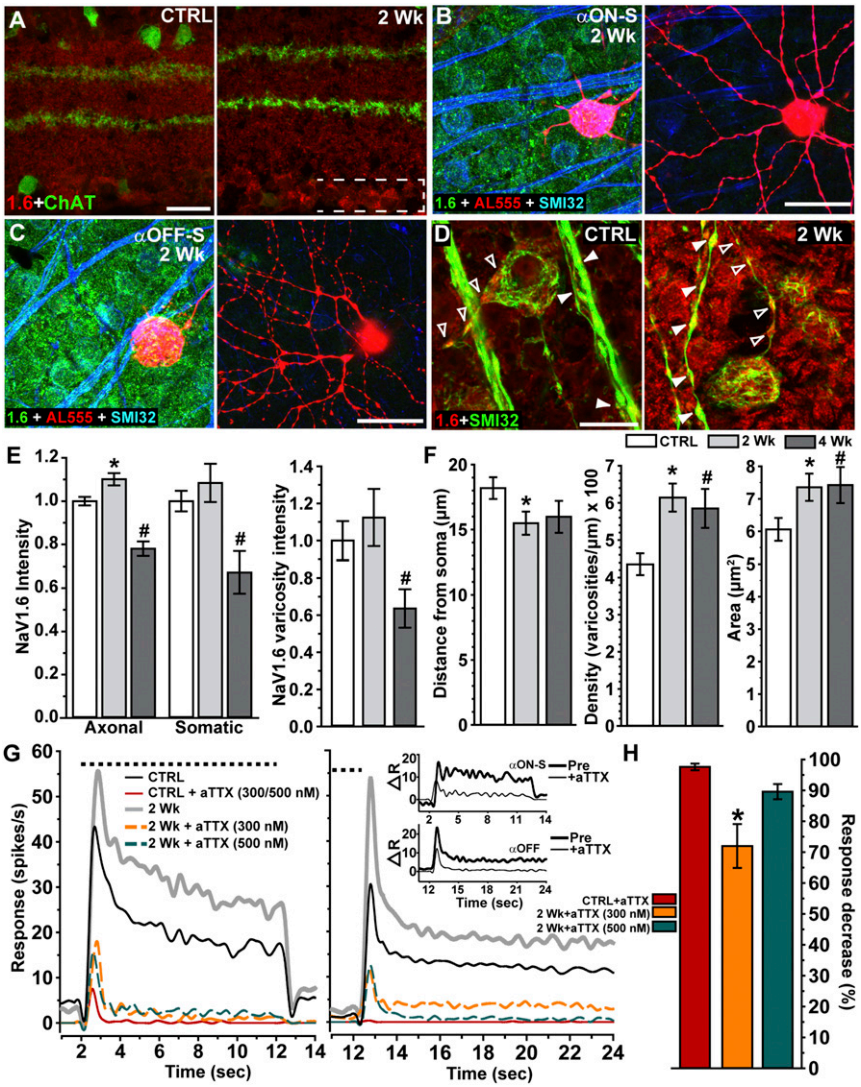

Fig. 5. Voltage-dependent channel NaV1.6 in axons contributes to enhanced light response. (*A*) Label for NaV1.6 (abbreviated as 1.6, red) shows increased localization specifically in the ganglion cell layer (bracketed) in 2-wk retina (*Right*) counterlabeled against ChAT for reference (green). (*B*, *Left*) An αON-S RGC following intracellular filling (AL555) in 2-wk retina labeled for NaV1.6 (green) and colabeled by SMI32 to show RGC cell bodies and axons (blue). (*B*, *Right*) Dendritic arbor of same αON-S RGC in the inner plexiform layer where NaV1.6 is nearly absent. (*C*, *Left*) An αOFF-S RGC following intracellular filling (AL555) in 2-wk retina labeled with same immunolabeling. (*C*, *Right*) Dendritic arbor of same αOFF-S RGC in the inner plexiform layer again shows little or no NaV1.6. (*D*) Intense NaV1.6 localization in RGC soma and in varicosities within both the proximal axon segment (open arrowheads) and in axon bundles (filled arrowheads) increases in 2-wk retina (*Right*). (*E*, *Left*) Quantification of NaV1.6 normalized to CTRL retina ($n = 3$) shows increased axonal localization in RGCs from 2-wk ($n = 3$) retinas ($^{*}P = 0.002$). This increase is transient, because both axonal and somatic localization decrease in 4-wk retina ($n = 2$) compared with CTRL ($^{\#}P \leq 0.001$). (*E*, *Right*) NaV1.6 in RGC varicosities increases slightly in 2-wk retina while significantly decreasing in 4-wk retina ($^{\#}P = 0.027$). (*F*) In 2-wk RGCs, varicosities distribute closer to the RGC soma (*Left*; $^{*}P = 0.026$), more densely within axons (*Center*; $^{*}P < 0.001$), and increase in maximal longitudinal area (*Right*; $^{*}P = 0.006$). Both density and area remain increased in 4-wk RGCs compared with CTRL ($^{\#}P \leq 0.022$). Measurements from the two varicosities most proximal to the RGC soma; $n = 14$–32 RGCs per eye and IOP period. (*G*) Mean response (spikes/s) to a 10-s light pulse (dashed line) for CTRL ($n = 7$) and 2-wk αON-S ($n = 6$) RGCs (*Left*) and CTRL ($n = 7$) and 2-wk ($n = 12$) αOFF-S/T RGCs (*Right*) before and after bath application of aTTX, a highly selective blocker of NaV1.6 (30). For both CTRL αON-S and αOFF-S/T RGCs, 300 and 500 nM aTTX were equally potent in suppressing the light response completely. For 2-wk αON-S and αOFF-S/T RGCs, 500 nM aTTX was required to achieve significant suppression; 300 nM was far less effective. (*Inset*) Difference in response to preferred light stimulus (spikes/s) between CTRL and 2-wk RGCs before and after application of 500 nM aTTX to each. (*H*) Mean efficacy of aTTX to suppress light calculated as percent decrease from predrug response for CTRL and for 2-wk αON-S and αOFF-S/T RGCs combined. For CTRL RGCs, 300 and 500 nM aTTX were equally effective in suppression (97% vs. 99%, $P = 0.99$), so the results were pooled. For 2-wk RGCs, 300 nM was only 72% effective, a significant difference from CTRL ($^{**}P < 0.001$), whereas 500 nM yielded nearly equivalent suppression. (Scale bars: *A* and *D*, 20 μm; *B* and *C*, 40 μm.) Data: mean ± SEM.

short-term, acute nature of the IOP elevation (peaking at +70%), which may have induced rapid adaption, or to the fact that our sample did not distinguish between directions of motion selectivity. Although the dendrites of αOFF-S RGCs did not change even after 4 wk of elevated IOP (Fig. S3), αOFF-T RGCs demonstrated reduced arbor size and total dendrite length after only 2 wk (Fig. S4). This is similar to the findings of Della Santina et al. (5), but contrary to those of Ou et al. (7), who described comparable pruning for αOFF-S and αOFF-T RGCs.

Dendritic pruning also did not depend on response polarity for RGCs identified morphologically in retinas of the DBA/2J mouse model of hereditary glaucoma (Figs. S5 and S6). This model presents significant loss of RGCs and their axons with age-related increases in IOP (21–23). We found that pruning was

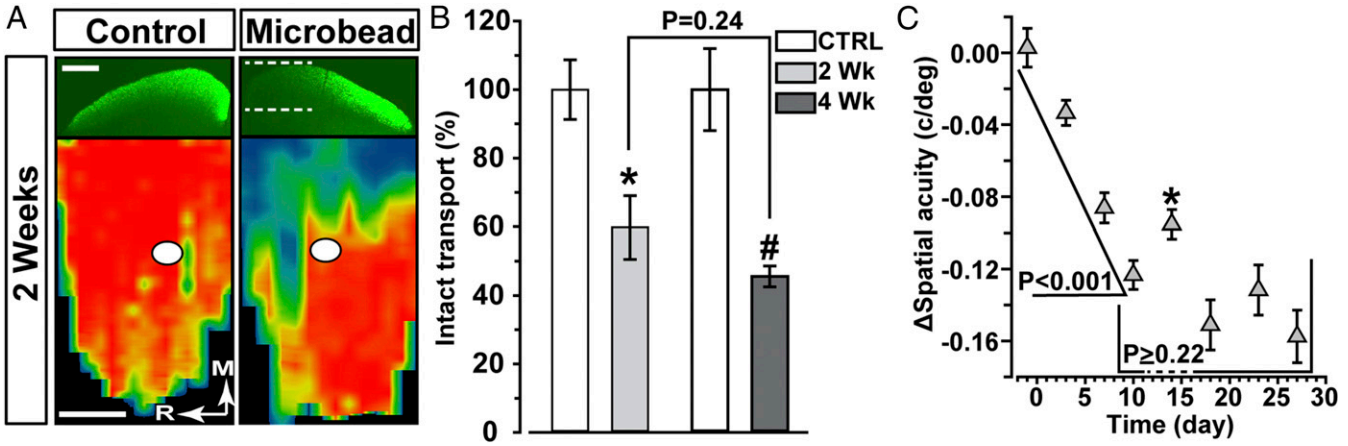

Fig. 6. Degradation of axonal transport and visual acuity pauses in progression. (*A*) Coronal sections through superior colliculus (SC) following intravitreal injection of cholera toxin B (CTB; green) into control and microbead-injected eyes of C57 mice. Two weeks of elevated IOP induced deficits in anterogradely transported CTB (dotted lines). (*Lower*) Retinotopic maps reconstructed from serial sections of SC with optic disk gap indicated (circles). Density of signal from transported CTB ranges from 0% (blue) to 50% (green) to 100% (red). Medial (M) and rostral (R) orientations indicated. (Scale bar: 500 μm.) (*B*) Fraction of SC with intact anterograde transport (defined by ≥70% CTB signal) normalized to CTRL eye levels following 2 ($n = 7$) and 4 ($n = 5$) wk of elevated IOP. Remaining transport at 2 wk is significantly lower than control (*$P = 0.018$). Although 4-wk transport is also significantly lower than the corresponding control ($^{\#}P = 0.008$), intact transport did not differ between 2 and 4 wk. (*C*) Difference in spatial frequency acuity in cycles per degree (c/deg) between control ($n = 35$) and microbead ($n = 35$) eyes increases significantly between ensuing measurements through 10 d ($P < 0.001$). Following a significant improvement at 2 wk (*$P = 0.02$), acuity did not decline past day 10 performance through nearly 4 wk ($P \geq 0.22$). Mean postinjection IOP for CTRL eyes was 14.28 ± 1.3, and that for microbead eyes 18.5 ± 1.7 ($P < 0.001$). Data: mean ± SEM.

significant at 10 mo of age and similar in magnitude among ON, OFF, and ON-OFF dendritic arbors, although we did not discriminate specific types. This result is consistent with an earlier comparison between RGCs in the DBA/2J retina (31).

An Axogenic Mechanism to Boost Excitation. We found that even with early dendritic pruning at 2 wk, no RGC type had a diminished response. Rather, each demonstrated an increased response to the preferred light (ON or OFF). For ON-OFF RGCs, the enhanced response was restricted to light onset (Fig. 3), just as dendritic pruning was restricted to the ON sublamina (Fig. 2). When normalized to their respective control group, each of the four RGC types examined had increased mean and peak firing rates and a faster response to the preferred light stimulus at 2 wk (Fig. 4). For αOFF-S RGCs the dendritic arbors remained intact (Fig. S1), although the light response did increase (Fig. 4). Interestingly, Ou et al. (7) also found an increased response, but with dendritic pruning. The response increase we report was transient for all RGCs, occurring by 2 wk of elevated IOP but decreasing to below control RGC levels by 4 wk (Fig. 4). This eventual decline is consistent with studies that followed the response for longer periods of IOP elevation (37, 38). Finally, the change in light response we document here took place on a backdrop of transiently enhanced excitability that included increased depolarization of the resting membrane potential with increased variability in membrane noise (Fig. 4).

Light-induced excitation of RGCs arises via glutamate from bipolar cell presynaptic ribbons that bind ionotropic glutamate receptors stabilized by PSD95 in RGC dendrites (24, 28). Bound glutamate depolarizes RGCs primarily through AMPA-sensitive receptors (Fig. S7*A*), thereby activating voltage-gated channels that propagate excitation (25, 26). The AMPA-driven contribution to the light response did not diminish after 2 wk of elevated IOP (Fig. S7 *B*–*D*), even with dendritic pruning in ON-OFF, αON-S, and αOFF-T RGCs. Only after 4 wk of elevation did the AMPA-mediated response show signs of decline, especially in ON-OFF and αOFF-T RGCs (Fig. S7*D*). This is commensurate with the decrease in levels of PSD95 in the inner plexiform layer we saw at 4 wk (Fig. S8 *A* and *B*). This result does not contradict reports of diminished PSD95 on individual RGC dendritic arbors before demonstrable pruning (5, 7). Our measurements reflect the entire inner plexiform layer with its great variety of glutamate receptor-expressing processes. Indeed for αON-S and ON-OFF RGCs, we found diminished response to AMPA delivered directly by puff pipette (Fig. S7 *E* and *F*). This measurement, reflecting the activity of postsynaptic receptors (26), decreased progressively between 2 and 4 wk of IOP elevation as did PSD95, even though dendritic pruning did not significantly change (Figs. 1 and 2).

Interestingly, 2 wk of IOP elevation increased immunolabeling for the presynaptic ribbon protein RIBEYE throughout the inner plexiform layer (Fig. S8 *C* and *D*). This effect too was transient, declining to control levels by 4 wk. The transient increase in RIBEYE at 2 wk contrasts with reduced numbers of synaptic ribbons found using a different marker (7). Colocalization with PSD95 did not change with elevated IOP but remained comparable with control levels (Fig. S8 *E* and *F*). Because PSD95 did not change at 2 wk, this may indicate multiple presynaptic ribbons for a given postsynaptic active zone. Increased RIBEYE in the inner retina may reflect a mechanism to stabilize the amplitude of AMPA receptor-mediated responses through presynaptic glutamatergic machinery in bipolar cell axons. Even as response amplitude persists due to presynaptic changes, ON and OFF RGC receptive fields should decrease in size as dendritic field area diminishes, effectively reducing the RGC sampling aperture in space. Recordings of the RGC spatial response to light in glaucoma models have confirmed this prediction (38). Perhaps more importantly, we found that isolating AMPA-mediated currents in RGCs while quenching voltage-gated sodium channels eradicated the transient increase in light response for all RGCs tested (Fig. S7 *A*–*D*). This result, coupled with diminished response to puffed AMPA (Fig. S7 *E* and *F*), demonstrates that conventional glutamatergic signaling between bipolar cells and RGCs does not underlie the increased light response. Similarly, we found that changes in inhibitory chloride currents also cannot explain the increased light response (Fig. S8 *G* and *H*), although the modestly diminished magnitude at 2 wk is consistent with early changes in GABAergic signaling observed in other glaucoma models (39, 40).

To explore further the voltage dependence of the increased light response, we examined the localization of NaV1.6, a voltage-gated sodium channel involved in action potential initiation and propagation (15). In the retina, NaV1.6 localizes predominantly in RGCs and their axons (41–44), a finding consistent with its biophysical function and one we now corroborate because localization in the inner plexiform layer was undetectable (Fig. 5 *B* and *C*). At 2 wk of IOP elevation, NaV1.6 increased in RGC axons, especially within varicosities that increased in size, density, and proximity to the RGC body (Fig. 5 *D*–*F*). This change coincided with the enhanced light response (Figs. 3 and 4). By 4 wk of elevation, NaV1.6 declined throughout the RGC to below control levels (Fig. 5*E*), again following precisely the transient pattern of the increased light response.

The NaV1.6 subunit produces a large persistent excitatory current that sustains generation of higher firing rates compared with other subunits (14). We propose that increased NaV1.6 in the RGC axon supports the enhanced light response at 2 wk of IOP elevation by bolstering excitation originating from remaining glutamatergic synapse in the dendritic arbor. Even the small (~5%) shift in RGC resting membrane potential that we observed (Figs. 3*C* and 4*J*) is sufficient to move axonal NaV1.6 from an inactivated to activated state (15). Furthermore, phosphorylated p38 mitogen-activated protein kinase, which we have shown increases in RGCs in glaucoma, directly activates NaV1.6 (45). Thus, increasing NaV1.6 in RGC axons should facilitate activation and increase firing, which could also explain the shorter response latency and increased membrane noise we observed at 2 wk (Fig. 4 *K* and *L*).

Activation of NaV channels close to cell bodies requires more depolarization (15). Because axonal varicosities are rich in mitochondria (46), increased size may hold more mitochondria, which would help support additional NaV1.6 activity. Finally, our physiological recordings using the NaV1.6-selective antagonist aTTX demonstrates a critical role for this subunit in driving action potential generation in response to the preferred light stimulus. For control RGCs its presence nearly eradicated the excitatory light response (Fig. 5*G*). For 2-wk αON-S and αOFF-S/T RGCs, although aTTX significantly suppressed the enhanced light response, even a 40% higher concentration left some residual response (Fig. 5*H*). This is consistent with the increased levels of NaV1.6 we observed for this IOP exposure (Fig. 5 *D* and *E*). Even so, we cannot exclude the possibility of additional voltage-dependent mechanisms contributing to enhancement, including the NaV1.2 subunit also expressed by RGCs (47).

Increased firing rate can improve correlated signaling between RGCs to help encode information embedded in a light stimulus (48, 49). We propose that RGCs that fail to do so may be more susceptible to early axonal degeneration, which is characteristic of glaucoma (23). Consistent with this idea, RGCs in mice lacking the transient receptor potential vanilloid-1 channel (*Trpv1*$^{-/-}$) not only have a higher threshold for excitation, but also undergo accelerated axon degeneration with elevated IOP (17, 18). Although transient increases in axonal NaV1.6 may promote RGC signaling, long-term changes could be deleterious for axons already challenged by glaucomatous stress. Where NaV1.6 colocalizes with the Na^+/Ca^{2+} exchanger in injured axons, its large persistent Na^+ current could reverse the exchanger, increasing intra-axonal Ca^{2+} to protease-activating levels (14, 50, 51). Increased persistent current through NaV1.6 channels contributes to neuronal hyperexcitability in epileptogenesis (30), which may be similar to the enhanced excitability we observed here (Fig. 4 *G*–*L*). That both the light response and Nav1.6 localization in axons diminished below control levels by 4 wk (Figs. 4 and 5*E*) suggests a delicate balance between the benefits of axogenic compensation and increased excitation and accelerated cytoskeletal degradation.

Although our results demonstrate that RGCs respond to IOP-related stress with a voltage-dependent mechanism to boost excitation, we cannot ascertain yet whether this mechanism is protective or ultimately deleterious to survival. Because the effect is transient, it is possible short-term elevations in IOP provide a preconditioning stimulus to slow progression. In the retina, although RGC dendritic arbors shrunk by 33–59% at 2 wk of elevation for αON-S, ON-OFF, and αOFF-T RGCs, pruning did not progress between 2 and 4 wk (Figs. 1 and 2 and Fig. S4). Similar persistence has occurred even with sharper elevations in IOP (7). Similarly, in the distal optic projection, we found that deficits in axonal anterograde transport to the SC did not progress between 2 and 4 wk of elevation (Fig. 6*B*). Finally, our measurements of spatial acuity using OKT demonstrate a dramatic and steady decline up to 2 wk of elevated IOP, at which point performance significantly improves and then stabilizes (Fig. 6*C*). Thus, the enhanced excitation in individual RGCs in response to disease-relevant elevations in IOP seems to translate to a broader influence on the optic projection as a whole.

Methods

Animals. The Vanderbilt University Medical Center Institutional Animal Use and Care Committee approved all experimental procedures. Young adult (2 mo) C57 mice (C57BL/6, male; Charles River Laboratory) were maintained in a 12-h light/dark cycle with standard rodent chow and water available ad libitum. We used unilateral microbead occlusion to elevate IOP in C57 mice, with the fellow eye receiving an equal volume saline injection as internal control (16–18). We measured IOP biweekly using rebound tonometry (Tono-Pen XL; Medtronic Solan), as described (16–18) (Fig. S9). For physiological recordings and intracellular filling, retinas were dissected under long-wavelength light (630 nm, 800 μW/cm^2; Ushio FND/FG). A subset of animals was bilaterally injected intravitreally with 1 μL of 0.5 mg cholera toxin subunit B (CTB) conjugated to Alexa Fluor 488 (Invitrogen). Intact transport within serial coronal superior colliculus sections was quantified (18, 23). For tissue required for immunolabeling of vertical sections and analysis of anterograde transport, mice were perfused transcardially with 4% paraformaldehyde.

Ex Vivo Retinal Preparation. Retinas were placed in the dark into a physiological chamber mounted on an upright microscope, maintained at 30 °C (TC-344B; Warner Instruments), and perfused (2 mL/min) with oxygenated bicarbonate buffered Ames' medium supplemented with 20 mM glucose (pH 7.4, Osm 290). For intracellular filling and patch-clamp recordings, we used fire-polished borosilicate glass pipettes containing (in mM) 125 K-gluconate, 10 KCl, 10 Hepes, 10 EGTA, 4 Mg-ATP, 1 Na-GTP, and 0.1 ALEXA 555 (Invitrogen) or 1 Lucifer Yellow (pH 7.35, Osm 285). Access resistance was ≤30 MΩ. Whole-cell RGC current and voltage signals were amplified (MultiClamp 700B; Molecular Devices) and digitized at a sampling rate of 10 kHz (Digidata 1550A; Molecular Devices). We measured resting membrane potential within 1 min after whole-cell configuration and calculated the coefficient of variation during a 5-s interval in current-clamp mode. Light responses were obtained using full-field light flashes of 365 nm (300 μW/cm^2, 3-s duration; Roithner Lasertechnik) generated by a light-emitting diode delivered through a shutter in the microscope condenser. The mouse retina produces a robust response to this wavelength based on the electroretinogram (52).

Following physiology, retinas were fixed overnight in 4% paraformaldehyde and immunolabeled for nonphosphorylated neurofilament H (SMI-32, 1:1,000; BioLegend) and ChAT (1:100; Millipore). All RGCs were from mid-peripheral retinal, 1,226 ± 35 μm from the optic nerve head, and equally distributed between superior vs. inferior and nasal vs. temporal quadrants without bias for the four types identified ($P \geq 0.10$). Confocal micrographs of all RGC dendritic arbors were obtained *en montage* using an Olympus FV-1000 inverted microscope and Sholl analysis of skeletonized arbors analyzed using ImageJ (Version 1.51i).

Optokinetic Tracking. Mice were placed on an elevated platform surrounded by four adjoining LCD monitors as described (53) (OptoMotry; CerebralMechanics Inc.). Visual response to drifting sine-wave gratings was measured through OKT reflex to the drifting sine-wave gratings of 100% contrast. Spatial frequency of the drifting grating was systematically adjusted to threshold depending on the animal's OKT response. Each grating was presented until a response (tracking) or no response (no tracking) was noted by the naïve experimenters.

Statistics. We performed one- or two-way ANOVAs (SigmaPlot 12.5; Systat). ANOVAs showing significance ($P < 0.05$) were followed by Tukey's (parametric)

or Dunn's (nonparametric) post hoc comparisons using independent samples (*t* tests). In some instances, when data distributions violated two or more of the assumptions of ANOVA (normality of residuals, equal variances, and independent sampling), we performed *t* tests or ANOVAs on ranked data. Before statistical analysis of dependent variables, we assessed the data for outliers, using Grubbs' test (GraphPad).

ACKNOWLEDGMENTS. Support was provided by NIH Grants R01EY024997 and P30EY008126; Training Grant in Vision Research T32 EY021833; Research to Prevent Blindness, Inc.; the Glaucoma Research Foundation; the Stanley Cohen Innovation Fund; and the Vanderbilt University Medical Center Cell Imaging Shared Resource core facility (Clinical and Translational Science Award Grant UL1 RR024975 from National Center for Research Resources).

1. Calkins DJ (2012) Critical pathogenic events underlying progression of neurodegeneration in glaucoma. *Prog Retin Eye Res* 31:702–719.
2. Almasieh M, Wilson AM, Morquette B, Cueva Vargas JL, Di Polo A (2012) The molecular basis of retinal ganglion cell death in glaucoma. *Prog Retin Eye Res* 31: 152–181.
3. Agostinone J, Di Polo A (2015) Retinal ganglion cell dendrite pathology and synapse loss: Implications for glaucoma. *Prog Brain Res* 220:199–216.
4. Shou T, Liu J, Wang W, Zhou Y, Zhao K (2003) Differential dendritic shrinkage of alpha and beta retinal ganglion cells in cats with chronic glaucoma. *Invest Ophthalmol Vis Sci* 44:3005–3010.
5. Della Santina L, Inman DM, Lupien CB, Horner PJ, Wong RO (2013) Differential progression of structural and functional alterations in distinct retinal ganglion cell types in a mouse model of glaucoma. *J Neurosci* 33:17444–17457.
6. El-Danaf RN, Huberman AD (2015) Characteristic patterns of dendritic remodeling in early-stage glaucoma: Evidence from genetically identified retinal ganglion cell types. *J Neurosci* 35:2329–2343.
7. Ou Y, Jo RE, Ullian EM, Wong RO, Della Santina L (2016) Selective vulnerability of specific retinal ganglion cell types and synapses after transient ocular hypertension. *J Neurosci* 36:9240–9252.
8. Sanes JR, Masland RH (2015) The types of retinal ganglion cells: Current status and implications for neuronal classification. *Annu Rev Neurosci* 38:221–246.
9. Baden T, et al. (2016) The functional diversity of retinal ganglion cells in the mouse. *Nature* 529:345–350.
10. Lin B, Wang SW, Masland RH (2004) Retinal ganglion cell type, size, and spacing can be specified independent of homotypic dendritic contacts. *Neuron* 43:475–485.
11. Coombs J, van der List D, Wang GY, Chalupa LM (2006) Morphological properties of mouse retinal ganglion cells. *Neuroscience* 140:123–136.
12. Trenholm S, Johnson K, Li X, Smith RG, Awatramani GB (2011) Parallel mechanisms encode direction in the retina. *Neuron* 71:683–694.
13. Schmidt TM, et al. (2014) A role for melanopsin in alpha retinal ganglion cells and contrast detection. *Neuron* 82:781–788.
14. Rush AM, Dib-Hajj SD, Waxman SG (2005) Electrophysiological properties of two axonal sodium channels, Nav1.2 and Nav1.6, expressed in mouse spinal sensory neurones. *J Physiol* 564:803–815.
15. Hu W, et al. (2009) Distinct contributions of Na(v)1.6 and Na(v)1.2 in action potential initiation and backpropagation. *Nat Neurosci* 12:996–1002.
16. Sappington RM, Carlson BJ, Crish SD, Calkins DJ (2010) The microbead occlusion model: A paradigm for induced ocular hypertension in rats and mice. *Invest Ophthalmol Vis Sci* 51:207–216.
17. Weitlauf C, et al. (2014) Short-term increases in transient receptor potential vanilloid-1 mediate stress-induced enhancement of neuronal excitation. *J Neurosci* 34: 15369–15381.
18. Ward NJ, Ho KW, Lambert WS, Weitlauf C, Calkins DJ (2014) Absence of transient receptor potential vanilloid-1 accelerates stress-induced axonopathy in the optic projection. *J Neurosci* 34:3161–3170.
19. Bleckert A, Schwartz GW, Turner MH, Rieke F, Wong RO (2014) Visual space is represented by nonmatching topographies of distinct mouse retinal ganglion cell types. *Curr Biol* 24:310–315.
20. Yoshida K, et al. (2001) A key role of starburst amacrine cells in originating retinal directional selectivity and optokinetic eye movement. *Neuron* 30:771–780.
21. John SW, et al. (1998) Essential iris atrophy, pigment dispersion, and glaucoma in DBA/2J mice. *Invest Ophthalmol Vis Sci* 39:951–962.
22. Inman DM, Sappington RM, Horner PJ, Calkins DJ (2006) Quantitative correlation of optic nerve pathology with ocular pressure and corneal thickness in the DBA/2 mouse model of glaucoma. *Invest Ophthalmol Vis Sci* 47:986–996.
23. Crish SD, Sappington RM, Inman DM, Horner PJ, Calkins DJ (2010) Distal axonopathy with structural persistence in glaucomatous neurodegeneration. *Proc Natl Acad Sci USA* 107:5196–5201.
24. Euler T, Haverkamp S, Schubert T, Baden T (2014) Retinal bipolar cells: Elementary building blocks of vision. *Nat Rev Neurosci* 15:507–519.
25. Kalbaugh TL, Zhang J, Diamond JS (2009) Coagonist release modulates NMDA receptor subtype contributions at synaptic inputs to retinal ganglion cells. *J Neurosci* 29: 1469–1479.
26. Sullivan SJ, Miller RF (2012) AMPA receptor-dependent, light-evoked D-serine release acts on retinal ganglion cell NMDA receptors. *J Neurophysiol* 108:1044–1051.
27. Pang JJ, Gao F, Wu SM (2003) Light-evoked excitatory and inhibitory synaptic inputs to ON and OFF alpha ganglion cells in the mouse retina. *J Neurosci* 23:6063–6073.
28. Morgan JL, Schubert T, Wong RO (2008) Developmental patterning of glutamatergic synapses onto retinal ganglion cells. *Neural Dev* 3:8.
29. tom Dieck S, Brandstätter JH (2006) Ribbon synapses of the retina. *Cell Tissue Res* 326: 339–346.
30. Hargus NJ, Nigam A, Bertram EH, 3rd, Patel MK (2013) Evidence for a role of Nav1.6 in facilitating increases in neuronal hyperexcitability during epileptogenesis. *J Neurophysiol* 110:1144–1157.
31. Jakobs TC, Libby RT, Ben Y, John SW, Masland RH (2005) Retinal ganglion cell degeneration is topological but not cell type specific in DBA/2J mice. *J Cell Biol* 171: 313–325.
32. Stevens B, et al. (2007) The classical complement cascade mediates CNS synapse elimination. *Cell* 131:1164–1178.
33. Morquette JB, Di Polo A (2008) Dendritic and synaptic protection: Is it enough to save the retinal ganglion cell body and axon? *J Neuroophthalmol* 28:144–154.
34. DeVries SH (1999) Correlated firing in rabbit retinal ganglion cells. *J Neurophysiol* 81: 908–920.
35. Völgyi B, Chheda S, Bloomfield SA (2009) Tracer coupling patterns of the ganglion cell subtypes in the mouse retina. *J Comp Neurol* 512:664–687.
36. Hu EH, Pan F, Völgyi B, Bloomfield SA (2010) Light increases the gap junctional coupling of retinal ganglion cells. *J Physiol* 588:4145–4163.
37. Pang JJ, Frankfort BJ, Gross RL, Wu SM (2015) Elevated intraocular pressure decreases response sensitivity of inner retinal neurons in experimental glaucoma mice. *Proc Natl Acad Sci USA* 112:2593–2598.
38. Chen H, et al. (2015) Progressive degeneration of retinal and superior collicular functions in mice with sustained ocular hypertension. *Invest Ophthalmol Vis Sci* 56: 1971–1984.
39. Zhou X, et al. (2017) Alpha7 nicotinic acetylcholine receptor agonist promotes retinal ganglion cell function via modulating GABAergic presynaptic activity in a chronic glaucomatous model. *Sci Rep* 7:1734.
40. Moon JI, et al. (2005) Changes in retinal neuronal populations in the DBA/2J mouse. *Cell Tissue Res* 320:51–59.
41. Caldwell JH, Schaller KL, Lasher RS, Peles E, Levinson SR (2000) Sodium channel Na(v) 1.6 is localized at nodes of ranvier, dendrites, and synapses. *Proc Natl Acad Sci USA* 97: 5616–5620.
42. Van Wart A, Matthews G (2006) Impaired firing and cell-specific compensation in neurons lacking nav1.6 sodium channels. *J Neurosci* 26:7172–7180.
43. Van Wart A, Matthews G (2006) Expression of sodium channels Nav1.2 and Nav1.6 during postnatal development of the retina. *Neurosci Lett* 403:315–317.
44. Mojumder DK, Wensel TG, Frishman LJ (2008) Subcellular compartmentalization of two calcium binding proteins, calretinin and calbindin-28 kDa, in ganglion and amacrine cells of the rat retina. *Mol Vis* 14:1600–1613.
45. Wittmack EK, Rush AM, Hudmon A, Waxman SG, Dib-Hajj SD (2005) Voltage-gated sodium channel Nav1.6 is modulated by p38 mitogen-activated protein kinase. *J Neurosci* 25:6621–6630.
46. Wang L, Dong J, Cull G, Fortune B, Cioffi GA (2003) Varicosities of intraretinal ganglion cell axons in human and nonhuman primates. *Invest Ophthalmol Vis Sci* 44:2–9.
47. Boiko T, et al. (2003) Functional specialization of the axon initial segment by isoform-specific sodium channel targeting. *J Neurosci* 23:2306–2313.
48. Zylberberg J, Cafaro J, Turner MH, Shea-Brown E, Rieke F (2016) Direction-selective circuits shape noise to ensure a precise population code. *Neuron* 89:369–383.
49. Barreiro AK, Ly C (2017) When do correlations increase with firing rates in recurrent networks? *PLoS Comput Biol*, 10.1371/journal.pcbi.1005506.
50. Stys PK, Waxman SG, Ransom BR (1992) Ionic mechanisms of anoxic injury in mammalian CNS white matter: Role of Na+ channels and Na(+)-Ca2+ exchanger. *J Neurosci* 12:430–439.
51. Craner MJ, Hains BC, Lo AC, Black JA, Waxman SG (2004) Co-localization of sodium channel Nav1.6 and the sodium-calcium exchanger at sites of axonal injury in the spinal cord in EAE. *Brain* 127:294–303.
52. Jacobs GH, Williams GA, Fenwick JA (2004) Influence of cone pigment coexpression on spectral sensitivity and color vision in the mouse. *Vision Res* 44:1615–1622.
53. Prusky GT, Alam NM, Beekman S, Douglas RM (2004) Rapid quantification of adult and developing mouse spatial vision using a virtual optomotor system. *Invest Ophthalmol Vis Sci* 45:4611–4616.